Journal of Materials Chemistry A

Accepted Manuscript

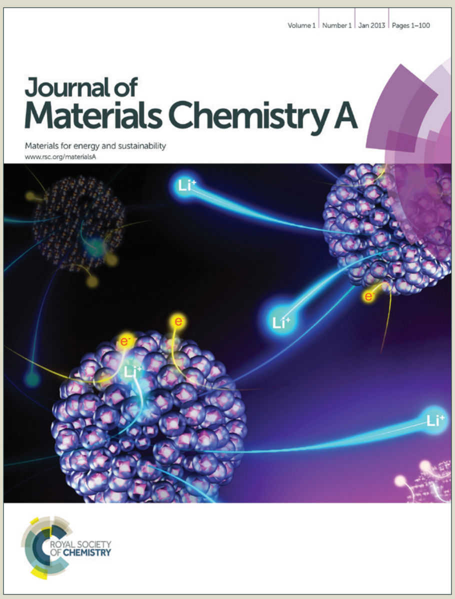

www.rsc.org/materialsA

Energy & Environmental Science

Journal of Materials Chemistry A

Dynamic Article Links►

Cite this: DOI: 10.1039/c0xx00000x

www.rsc.org/xxxxxx

COMMUNICATION

Highly Efficient Organic Solar Cells Using Solution-Processed Active Layer with Small Molecule Donor and Pristine Fullerene

Hao-Wu Lin,*[a] Jung-Hao Chang,[a] Wei-Ching Huang,[a] Yu-Ting Lin,[a] Li-Yen Lin,[b] Francis Lin,[b] Ken-Tsung Wong,*[b,c] Hsiao-Fang Wang,[d] Rong-Ming Ho[d] and Hsin-Fei Meng[e]

Received (in XXX, XXX) XthXXXXXXXXX 20XX, Accepted Xth XXXXXXXXX 20XX
DOI: 10.1039/b000000x

A new strategy has been successfully established to realize high efficiency small molecule organic solar cells with solution-processed active layer composing of small organic molecule as donor and pristine C_{70} as acceptor. Using 1,2-dichlorobenzene as solvent, the homogeneous donor/C_{70} blending active layer can be effectively formed either by spin- or bar-coating techniques. This method delivers organic solar cells with high power conversion efficiencies up to 5.9%.

Introduction

Organic solar cells (OSCs) are emerging as a clean and competitive renewable energy resource due to their unique features including low-cost manufacturing, light weight, and mechanical flexibility. Among all OSCs, solution-processed organic bulk heterojunction (BHJ) solar cells, which consist of a phase-separated blend of a conjugated polymer as electron donor and a fullerene derivative as electron acceptor have gained tremendous successes.[1-11] Nevertheless, solution-processed OSCs utilizing small molecules as electron donors and acceptors received relatively less attention prior to 2006, but have shown growing interests recently.[12-19] Molecular donors offer the facile solution-processing capability associated with polymers, yet present specific advantages such as structural definition, easy synthesis and purification. Recently, solution-processed small molecule organic solar cells (SMOSCs) with power conversion efficiency (PCE) exceeding 8% have been successfully demonstrated.[19-21] To increase the solubility in solvent or to mimic the morphology control strategies developed in polymer-based solar cells, small molecule donors and acceptors suitable for solution process were typically modified with long alkyl chains. However, the introductions of alkyl chains onto the conjugated backbone usually require more synthetic steps which may raise the cost and energy in material production. Furthermore, long alkyl chains make these compounds hard to purify by sublimation, which is believed to be the best way of producing high purity materials for organic electronics. An alternative could be beneficial to achieve efficient solution-processed SMOSCs if pristine donor and acceptor can be directly utilized without tedious synthesis and/or purification. This approach will potentially pave an effective way of producing low-cost light-harvesting devices. To this end, we have systematically investigated appropriate methods to fabricate bulk heterojunction composites of donors without long alkyl groups and pure C_{70}. For fair comparisons, the donors used in this report are molecules featuring with donor-acceptor-acceptor (D-A-A) configuration, which were previously utilized in vacuum-processed SMOSCs, where C_{70} was used as acceptor. By carefully tuning the material compositions and solvents as well as deposition methods, solution-processed SMOSCs with high power efficiencies approaching to 6% have been successfully achieved. Our current results represent one major step forward in the development of cost-effective and low energy consumption SMOSCs.

[a]*Department of Materials Science and Engineering, National Tsing Hua University, No. 101, Section 2, Kuang-Fu Road, Hsinchu, Taiwan 30013. E-mail: hwlin@mx.nthu.edu.tw*
[b]*Department of Chemistry, National Taiwan University,* [c]*Institute of Atomic and Molecular Sciences, Academia Sinica, No.1, Section 4, Roosevelt Road, Taipei, Taiwan 10617. E-mail: kenwong@ntu.edu.tw*
[d]*Department of Chemical Engineering, National Tsing Hua University, Hsinchu, Taiwan 30013.*
[e]*Institute of Physics, National Chiao Tung University, Hsinchu, Taiwan 30013.*

Experimental

Device fabrication

Before thin film deposition, indium tin oxide (ITO) coated glass substrates (sheet resistance ~ 10 Ω/sq) were cleaned in an ultrasonic bath with de-ionized water, acetone, and methanol for 15 min, respectively. The MoO_3, CsF, Ca layers were deposited onto ITO glass substrate in high vacuum chamber with base pressure of ~8 x10^{-7} Torr, and the deposition were performed at a rate of 1~2 Å/s with the substrates held at room temperature. The sol-gel films of ZnO were spin-coated onto ITO glass substrates from a zinc acetate solution (7.3 mg/mL) in 96% 2-methoxy ethanol and 4% ethanolamine, and then annealed in air at 150 ^{o}C for 5 min. A blend solution of solar active donors and fullerene (purchased from Nano-C) were prepared using chloroform, chlorobenzene (CB), 1,2-dichlorobenzene (DCB) or 1,2,4-trichlorobenzene (TCB) as solvent with different ratios and a total concentration ranging from 12 to 30 mg/mL. The solution was stirred for 4 hrs at 65 ^{o}C, and cooled down to ambient temperature before casting. The active layers were spin-coated or bar-coated on pre-treated substrate in a glove box under the anhydrous nitrogen atmosphere. For the spin-casted thin films, the layer thickness was controlled by spin speed (800 to 3000 rpm) and solute concentration. For the bar-coated thin films, the layer thickness was controlled by bar speed (60 to 450 mm/s) and solute concentration. The samples were then transferred to a vacuum chamber for the sequential deposition of donor neat films, MoO_3, and top Ag electrode. Devices were encapsulated using a

UV-cured sealant (*Everwide Chemical Co.*, *Epowide EX*) and a cover glass under the anhydrous nitrogen atmosphere after fabrication and were measured in air. The active area of the cells had an average size of 5 mm^2 (intersect area between Ag cathode and ITO anode) and were carefully measured device-by-device using calibrated optical microscope. The thin films for TEM bright-field top-view investigation were prepared by immersing the glass/PEDOT:PSS/thin-films samples into deionized water. After dissolution of PEDOT:PSS, thin-films floated onto the water surface and were transferred to a TEM grid.

Characteristics measurements

Current density-voltage characteristics were measured with a Source Meter *Keithley* 2400 under AM 1.5G simulated solar illumination from a xenon lamp solar simulator (*Abet Technologies*). The incident light intensity was calibrated as 100 mW/cm^2 using a NREL-traceable KG5 filtered Si reference cell. The external quantum efficiency (EQE) spectra were taken by illuminating chopped monochromatic light with a continuous-wave bias white light (from halogen lamp, intensity ~100 mW/cm^2) on the solar cells. The photocurrent signals were extracted with lock-in technique using a current preamplifier (*Stanford Research System*) followed by a lock-in amplifier (*AMETEK*). The EQE measurement is fully computer controlled and the intensity of monochromatic light is carefully calibrated with NIST-traceable optical power meter (*Ophir Optronics*). Thicknesses and extinction coefficients (k) of the thin films were determined using spectroscopic ellipsometry (*J. A. Woollam Inc. V-VASE*). Atomic force microscopy (AFM) images were analyzed with a *Bruker Dimension Icon® Atomic Force Microscope* operating in tapping mode. Transmission electron microscopy (TEM) images were analyzed with a *JEOL JEM-1200x* transmission electron microscope (accelerating voltage: 120 keV).

Results

Along the line of conventional approach, hexyloxy groups were introduced onto a well-performed D-A-A donor (**DTDCTP**)[22, 23] to give the modified donor **DP6DCTP** (Scheme 1) with improved solubility in organic solvents. In conjunction with typical solution-processed acceptor [6,6]-phenyl-C_{61}-butyric acid methyl ester ($PC_{61}BM$), BHJ SMOSCs using **DP6DCTP**:$PC_{61}BM$ as active layer were fabricated using spin-casting technique. However, the achieved PCEs of 0.35~0.56% (see Fig. S1, in Supporting Information (SI)) are far from satisfactory as compared to those of contemporary results.

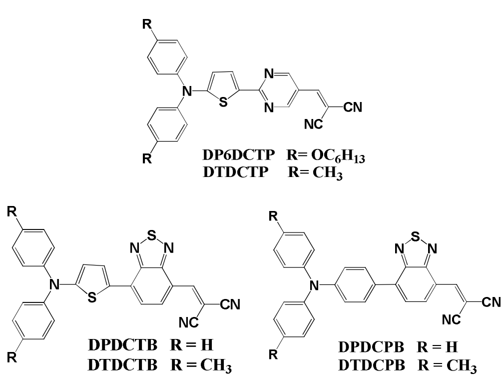

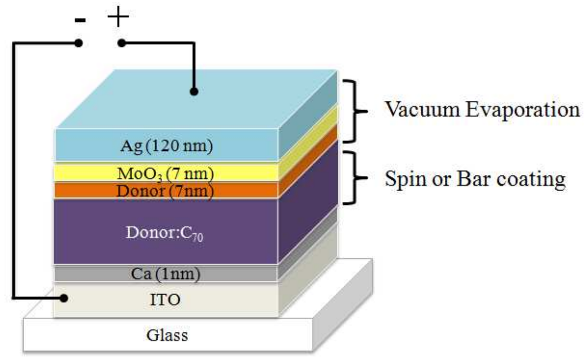

Scheme 1 Molecular structures of **DP6DCTP**, **DTDCTP**, **DPDCPB**, **DTDCPB**, **DPDCTB**, **DTDCTB**and the optimized device structure in this study.

The long alkyl groups in **DP6DCTP** is aiming to increase the solubility for solution process. However, these non-conjugated hydrocarbons may increase the spacial occupation and therefore decrease the chromophore density in the active layer. Fortunately, we found the parent donor **DTDCTP** performed good solubilities (> 20 mg/mL) in various solvents such as chlorobenzene, 1,2-dichlorobenzene, and chloroform, which will be sufficient to form a strong absorbing layer with an adequate thickness (50~100 nm) for efficient light-harvesting. Encouraging by the high solubility of **DTDCTP**, SMOSCs with spin-coated **DTDCTP**:$PC_{61}BM$ (1:1) as the active layer configured into an inverted cell structure were fabricated. We adopted inverted cell structure since it possesses several advantages such as the replacement of the low T_g materials (ex: BCP) with hole-transporting metal oxide (ex: MoO_3) as optical spacer between active layer and metal electrodes[13, 24, 25] and/or the possibility to insert a donor neat film above the mixed active layer to facillitate hole-transporting/extracting. One advantage of our donors is able to from a homogeneous neat film upon vacuum sublimation. Thus, a 7-nm donor neat film was introduced here, which can also increase a small portion of light absorption and thus contribute some photocurrents. Several modified transparent indium tin oxide (ITO) electrodes such as ITO (device A), ITO/sol-gel ZnO (device B), ITO/CsF (device C), and ITO/Ca (device D) were used as cathodes where MoO_3/Ag was used as anode. The J-V characteristics and EQE spectra of devices A~D are shown in **Fig. 1**. Clearly, bare ITO without additional treatment (device A) shows the lowest PCE. In addition, the V_{oc} of device B was lowered down to 0.74 V, which was ascribed to high dark current owing to the high surface roughness (R_{max} ~ 20 nm measured by atomic force microscopy) of the sol-gel ZnO[26, 27]. In contrast, devices C and D with ITO/CsF and ITO/Ca as cathodes show higher and comparable PCEs of 1.4 and 1.5%, respectively. As a result, ITO/Ca was selected as cathode for our further studies. The inverted structure configured as: ITO/Ca/mixed layer/donor layer/MoO_3/Ag (Scheme 1), where the mixed layer was formed by spin-coating, and then thin donor layer/ MoO_3/Ag layers were vacuum deposited sequentially.

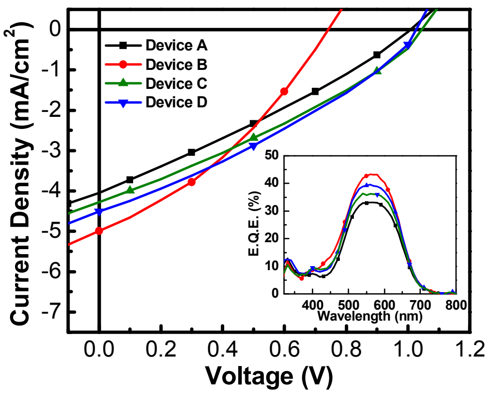

Figure 1. *J*–V characteristics (under 1 sun, AM 1.5G illumination) and EQE spectra (inset) of the devices with the following structures: ITO/none (Device A), sol-gel ZnO (Device B), CsF (Device C) and Ca (Device D)/**DTDCTP**:$PC_{61}BM$ (1:1 by weight, 40 nm)/ **DTDCTP** (7 nm)/MoO_3 (30 nm)/Ag (120 nm).

The acceptor $PC_{61}BM$ in device D was further replaced with [6,6]-phenyl-C_{71}-butyric acid methyl ester ($PC_{71}BM$), which exhibits similar electronic properties as $PC_{61}BM$, but performs a higher extinction coefficient (*k*) in the blue and cyan region (**Fig. 2** inset). The effect of **DTDCTP**:$PC_{71}BM$ blending layer thickness (50~70 nm) on the device characteristics was further investigated (Fig. S2 in SI). The best cell (device E) with a thin (50 nm) **DTDCTP**:$PC_{71}BM$ layer exhibits a J_{sc} of 7.46 mA/cm^2, V_{oc} of 1.05 V, FF of 30% and an overall PCE of 2.4% (**Fig. 2**). The thickness dependent device performances suggest that the bimolecular recombination becomes a dominate factor in these devices.

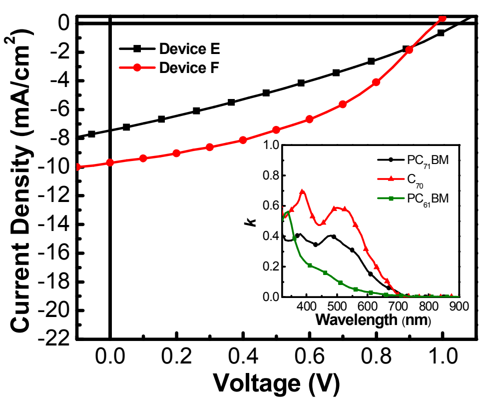

Figure 2. *J*–V characteristics (under 1 sun, AM 1.5G illumination) of the devices with different acceptors. The device structures are ITO/Ca (1 nm)/**DTDCTP**:$PC_{71}BM$ (Device E, 1:2 by weight, 50 nm) and **DTDCTP**:C_{70} (Device F, 1:1.5 by weight, 50 nm)/**DTDCTP** (7 nm)/MoO_3 (7 nm)/Ag (120 nm), inset Extinction coefficients of $PC_{71}BM$, C_{70} and $PC_{60}BM$.

In spite of the solution processibility of $PC_{61}BM$ and $PC_{71}BM$, pristine C_{70} exhibits highest *k* in the visible spectrum region (**Fig. 2** inset). As a consequence, C_{70} should be the best candidate serving as the acceptor component to pair with **DTDCTP** with feasible solution-process for fabricating efficient SMOSCs, as we have achieved in vacuum-deposited devices.[22] However, this new idea is highly challenging due to the low solubility of C_{70} in common organic solvents and poor film-forming ability. Propitiously, we have found that DCB is able to dissolve adequate amount of **DTDCTP** and C_{70} (greater than 20 mg/mL) for spin-casting. To be our surprise, the efficiencies of spin-casted **DTDCTP**:C_{70} cells are largely enhanced. It is noteworthy that a trade-off between the increase of photon harvesting (thicker films) and the decrease of carrier recombination (thinner films) are found in the **DTDCTP**:C_{70} based devices with various thicknesses of the blending layer. This trade-off effect clearly results in the monotonic increase of J_{SC} values and decrease of FF values as the mixed layer thickness increases (see Fig. S3 in SI). The optimized device (device F) with a **DTDCTP**:C_{70} (1:1.5) mixed layer thickness of ca. 50 nm shows an impressive PCE of 4.0% (**Fig. 2**), which is nearly 2-fold increment compared to the best **DTDCTP**:$PC_{71}BM$ cell. Obviously, this result indicates that efficient SMOSCs with solution-processed pristine C_{70} as electron acceptor together with small molecule as electron donor can be feasibly achieved. The combination of small molecule donor and pristine fullerene not only improves the cell performance but also provides a significant advantage of simplicity for molecular design and synthesis. To the best of our knowledge, our current method is new for giving efficient (PCE > 3%) solution-processed BHJ SMOSCs.

We believe that the performance enhancement should not be only limited to this specific case, but may generally apply to other small molecule systems. Along this line, a systematic study was conducted with this newly developed protocol using a series of D-A-A donors, namely, **DPDCPB**, **DTDCPB**, **DPDCTB**, and **DTDCTB** (Scheme 1). These small molecules were originally designed for vacuum-processed high efficiency SMOSCs.[28-31] The ratio of donor:C_{70} and the thickness of spin-coated active layer have been carefully tuned (Fig. S4~7, Table S4~7 in SI). **Fig. 3(a)** shows the *J*-V characteristics of the optimized spin-casted devices and the data are summarized in Table 1. The optimized devices show high efficiencies up to 4.1% (device G: **DPDCPB**:C_{70}), 5.4% (device H: **DTDCPB**:C_{70}), 3.7% (device I: **DPDCTB**:C_{70}), and 5.2% (device J: **DTDCTB**:C_{70}).

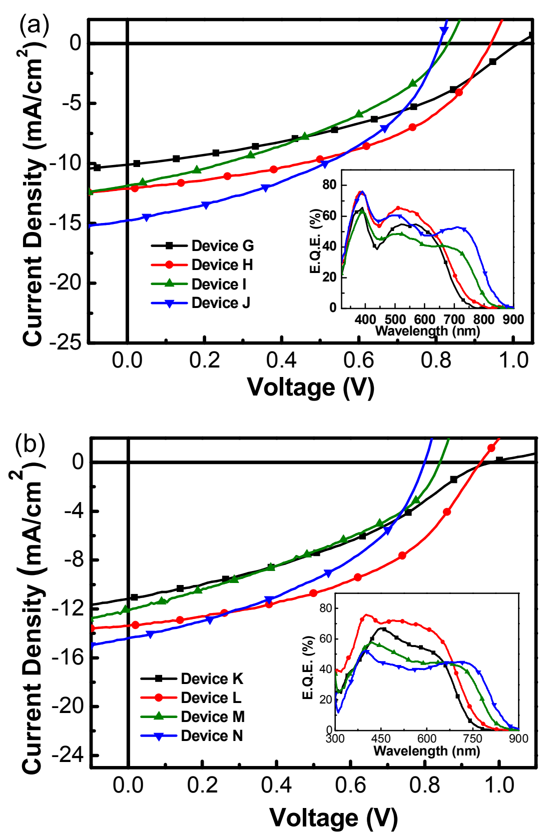

Figure 3. *J*–V characteristics (under 1 sun, AM 1.5G illumination) and

EQE spectra (inset) of solar cells fabricated from **DPDCPB**(Device G, K), **DTDCPB**(Device H, L), **DPDCTB**(Device I, M), and **DTDCTB**(Device J, N) by (a) spin-coating and (b) bar-coating processes. The device structures are: ITO/Ca (1 nm)/donor:C_{70}/donor (7 nm)/MoO_3 (7 nm)/Ag (120 nm).

Table 1. Performance parameters of the optimized devices under AM 1.5G simulated solar illumination at intensity of 100 mW/cm^2.

Device type	V_{OC} (V)	J_{SC} (mA/cm^2)	FF (%)	η (%)
Device F: **DTDCTP**:C_{70} (1:1.5)[a]	0.98	9.7	42	4.0
Device G: **DPDCPB**:C_{70} (1:1.5)[a]	1.01	10.9	40	4.1
Device H: **DTDCPB**:C_{70} (1:1.5)[a]	0.94	12.1	47	5.4
Device I: **DPDCTB**:C_{70} (1:2.0)[a]	0.83	11.9	37	3.7
Device J: **DTDCTB**:C_{70} (1:1.8)[a]	0.81	14.8	43	5.2
Device K: **DPDCPB**:C_{70} (1:2.2)[b]	0.98	11.1	36	3.9
Device L: **DTDCPB**:C_{70} (1: 2.2)[b]	0.95	13.4	46	5.9
Device M: **DPDCTB**:C_{70} (1: 2.2)[c]	0.85	12.1	37	3.8
Device N: **DTDCTB**:C_{70} (1: 2.2)[b]	0.82	14.5	43	5.1

[a]Active-layer thin films were cast from 1,2-dichlorobenzene solution by spin-coated process. [b]Active-layer thin films were cast from 1,2-dichlorobenzene and 1,2,4-trichlorobenzene mixture solutions (1:1 by volume) by bar-coated process. [c]Active-layer thin films were cast from 1,2-dichlorobenzene and chlorobenzene mixture solutions (7:3 by volume) by bar-coated process.

In a well-optimized cell without carrier accumulation and interfacial recombination, the V_{oc} value of the device is usually correlated to the energy difference between the highest occupied molecular orbital (HOMO) level of the donors and the lowest unoccupied molecular orbital (LUMO) level of fullerene.[32] In this study, the differences in V_{oc} values of spin-casted cells are indeed related to the HOMO levels of donors as previously observed in vacuum-deposited ones.[29] On the other hand, the J_{sc} values depend on the bandgaps and extinction coefficients of these donors, which can be clearly verified in the EQE spectra. As shown in inset of **Fig. 3(a)**, the EQE spectra of both device I and device J exhibit broad responses covering from UV to near-infrared (IR) region. In particular, device J shows high EQE values of ~50% from visible to near-IR wavelength range and extends photoresponse up to 800 nm, resulting in a very high J_{sc} of 14.8 mA/cm^2 and a PCE exceeding 5%. Moreover, through striking a balance between the photovoltage and photocurrent,[29] device H achieves the highest overall PCE of 5.4% with a V_{oc} of 0.94 V, a J_{sc} of 12.1 mA/cm^2 and a FF of 47%. Compared to vacuum-deposited cell in our previous reports,[22, 28, 29] the V_{oc} values of solution-processed devices are almost identical. However, the J_{sc} and FF values of spin-casted cells were ~10% lower, which is owing to the simpler device structure (i.e. planar mixed heterojunction in vacuum-deposited devices vs. bulk heterojunction in spin-casted devices). As a result, the solution-processed devices achieve ~80% PCE of which the vacuum-deposited devices counterparts can obtain. In addition, the FF values of these spin-casted devices range from 36 to 47%, which are on the low side of modern organic solar cells as compared to those utilizing polymers or tailor-made small molecules as electron donors. This could be ascribed to defective carrier transportation pathways[33] due to the lack of well-ordered D/A nano structures, which were evidenced in the atomic force microscopy images of the spin-coated films (Fig. S8). Nevertheless, our new results are quite promising in terms of simplicity and production costs.

In addition to spin-coating method, bar-coating technique was also adopted to fabricate active layer for SMOSCs. The bar-coating technique has already been used in the fabrications of organic light emitting device and polymer solar cell with favorable advantages such as better film formation and nearly 100% material utilization.[34, 35] With DCB as solvent and the donor/acceptor ratio set to 1:2.2. These devices showed comparable PCEs to those of devices using spin-cast technique (Fig. S9, Table S8 in SI). One of the attractive benefits from solution-processed SMOSCs is the space for improving PCE by the manipulation of the active layer morphology. Among various treatments on the active layer for better PCEs, the *in-situ* solvent-annealing has its merit of simplicity. Therefore, we adopted a co-solvent treatment in our bar-coated SMOSCs, allowing an extra ~20% improvement of performance in all benzothiadiazole-based D-A-A donors devices after the solvent composition optimization (see Fig. S10~S11 and Table S9~S10 in SI). The *J*-V characteristics of the optimized bar-coated devices are depicted in **Fig. 3(b)** and the data are summarized in Table 1, which are comparable or even better than those of spin-casted devices in spite of the similar bar-coated AFM images (Fig. S12) of the active layers were obtained. However, D/A segregation domains size of ~ 20 nm can be observed in the AFM phase images, which led to higher PCEs in **DTDCPB**- and **DTDCTB**-based devices as compared to those of **DPDCPB**- and **DPDCTB**-based ones. The best bar-coated devices show PCEs of 3.9% (device K: **DPDCPB**:C_{70}), 5.9% (device L: **DTDCPB**:C_{70}), 3.8% (device M: **DPDCTB**:C_{70}) and 5.1% (device N: **DTDCTB**:C_{70}). Interestingly, the characteristics such as V_{oc}, J_{sc} and EQE spectra of optimized devices show similar trends regardless of the different thin-film formation methods. Among them, the bar-coated devices employed **DTDCPB** as electron donor combining with C_{70} as acceptor (device L) show the best performance with a V_{oc} of 0.95, a J_{sc} of 13.4 mA/cm^2,a fill factor of 46% and a PCE as high as 5.9%. This result is consistent with our previous observations from the vacuum-processed and spin-casted SMOSCs. More importantly, ~90% efficiency of vacuum-deposited cell (PCE = 6.8%) using the same donor and acceptor now can be achieved with this newly developed method.

Because the AFM results only provide the information of surface morphology, we then further probed the bulk morphology by using TEM. Three samples were prepared: (a) DTDCPB:C_{70} (1:1.5) thin film spin-casted from a DCB solution, (b) DTDCPB:C_{70} (1:2.2) thin film bar-coated from a DCB solution, and (c) DTDCPB:C_{70} (1:2.2) thin film bar-coated from a DCB and TCB (1:1 by volume) mixed solution. These samples are corresponding to the most efficient devices (devices H, S_{21}, and L) obtained by spin-coating and bar-coating method respectively. The results are shown in Fig. S13. Both D/A blended films casted from a DCB solution by spin- and bar-coated process exhibited a less distinctly resolved domain structure and larger features as compared to that of the thin film casted from a DCB/TCB mixed solution. The distinct domain and smaller domain size formation in the thin film casted from DCB/TCB mixed solution could assist both exciton separation and carrier transportation, leading to the highest device performance in this work.

Conclusions

In summary, an new strategy for the realization of SMOSCs with solution-processed BHJ active layer composing of organic compounds without long alkyl substitutions as donor and pristine C_{70} as acceptor has been successfully established. The donor/C_{70} blending active layer can be effectively formed either by spin-coating or bar-coating techniques. This new method can be generally applied to various organic D-A-A donors, delivering SMOSCs with high PCEs up to 5.9%, which is about 90% of the best device fabricated by the vacuum deposition technique. We believe that the works accomplished in this paper can facilitate the development of new organic molecules as low-cost donor materials and provide new guidelines for the fabrication of highly efficient solution-processed organic photovoltaics.

Acknowledgements

We thank National Science Council of Taiwan and the Low Carbon Energy Research Center, National Tsing-Hua University, for financial support.

Notes and references

1. J. You, L. Dou, K. Yoshimura, T. Kato, K. Ohya, T. Moriarty, K. Emery, C. C. Chen, J. Gao, G. Li and Y. Yang, *Nat Commun.*, 2013, **4**, 1446.
2. Z. Tan, W. Zhang, Z. Zhang, D. Qian, Y. Huang, J. Hou and Y. Li, *Adv. Mater.*, 2012, **24**, 1476.
3. M. S. Su, C. Y. Kuo, M. C. Yuan, U. S. Jeng, C. J. Su and K. H. Wei, *Adv. Mater.*, 2011, **23**, 3315.
4. C. Duan, F. Huang and Y. Cao, *J. Mater. Chem.*, 2012, **22**, 10416.
5. T. Y. Chu, J. Lu, S. Beaupre, Y. Zhang, J. R. Pouliot, S. Wakim, J. Zhou, M. Leclerc, Z. Li, J. Ding and Y. Tao, *J. Am. Chem. Soc.*, 2011, **133**, 4250.
6. Z. He, C. Zhong, X. Huang, W. Y. Wong, H. Wu, L. Chen, S. Su and Y. Cao, *Adv. Mater.*, 2011, **23**, 4636.
7. H. Zhou, L. Yang, A. C. Stuart, S. C. Price, S. Liu and W. You, *Angew. Chem., Int. Ed.*, 2011, **50**, 2995.
8. C. E. Small, S. Chen, J. Subbiah, C. M. Amb, S.-W. Tsang, T. H. Lai, J. R. Reynolds and F. So, *Nat. Photonics*, 2012, **6**, 115.
9. T. Yang, M. Wang, C. Duan, X. Hu, L. Huang, J. Peng, F. Huang and X. Gong, *Energy Environ. Sci.*, 2012, **5**, 8208.
10. J. M. Szarko, J. Guo, Y. Liang, B. Lee, B. S. Rolczynski, J. Strzalka, T. Xu, S. Loser, T. J. Marks, L. Yu and L. X. Chen, *Adv. Mater.*, 2010, **22**, 5468.
11. B. Walker, J. Liu, C. Kim, G. C. Welch, J. K. Park, J. Lin, P. Zalar, C. M. Proctor, J. H. Seo, G. C. Bazan and T.-Q. Nguyen, *Energy Environ. Sci.*, 2013, **6**, 952.
12. T. Bura, N. Leclerc, S. Fall, P. Leveque, T. Heiser, P. Retailleau, S. Rihn, A. Mirloup and R. Ziessel, *J. Am. Chem. Soc.*, 2012, **134**, 17404.
13. H. Y. Lin, W. C. Huang, Y. C. Chen, H. H. Chou, C. Y. Hsu, J. T. Lin and H. W. Lin, *Chem. Commun.*, 2012, **48**, 8913.
14. H. Tanaka, Y. Abe, Y. Matsuo, J. Kawai, I. Soga, Y. Sato and E. Nakamura, *Adv. Mater.*, 2012, **24**, 3521.
15. J. Huang, C. Zhan, X. Zhang, Y. Zhao, Z. Lu, H. Jia, B. Jiang, J. Ye, S. Zhang, A. Tang, Y. Liu, Q. Pei and J. Yao, *ACS Appl. Mater. Interfaces*, 2013, **5**, 2033.
16. T. S. van der Poll, J. A. Love, T. Q. Nguyen and G. C. Bazan, *Adv. Mater.*, 2012, **24**, 3646.
17. X. Xiao, G. Wei, S. Wang, J. D. Zimmerman, C. K. Renshaw, M. E. Thompson and S. R. Forrest, *Adv. Mater.*, 2012, **24**, 1956.
18. A. K. Kyaw, D. H. Wang, V. Gupta, J. Zhang, S. Chand, G. C. Bazan and A. J. Heeger, *Adv. Mater.*, 2013, **25**, 2397.
19. J. J. Jasieniak, B. B. Y. Hsu, C. J. Takacs, G. C. Welch, G. C. Bazan, D. Moses and A. J. Heeger, *ACS Nano*, 2012, **6**, 8735.
20. J. Zhou, Y. Zuo, X. Wan, G. Long, Q. Zhang, W. Ni, Y. Liu, Z. Li, G. He, C. Li, B. Kan, M. Li and Y. Chen, *J. Am. Chem. Soc.*, 2013, **135**, 8484.
21. V. Gupta, A. K. K. Kyaw, D. H. Wang, S. Chand, G. C. Bazan and A. J. Heeger, *Sci. Rep.*, 2013, **3**, 1965.
22. S. W. Chiu, L. Y. Lin, H. W. Lin, Y. H. Chen, Z. Y. Huang, Y. T. Lin, F. Lin, Y. H. Liu and K. T. Wong, *Chem. Commun.*, 2012, **48**, 1857.
23. H. W. Lin, S. W. Chiu, L. Y. Lin, Z. Y. Hung, Y. H. Chen, F. Lin and K. T. Wong, *Adv. Mater.*, 2012, **24**, 2269.
24. D. W. Zhao, P. Liu, X. W. Sun, S. T. Tan, L. Ke and A. K. K. Kyaw, *Appl. Phys. Lett.*, 2009, **95**, 153304.
25. C. Y. Jiang, X. W. Sun, D. W. Zhao, A. K. K. Kyaw and Y. N. Li, *Sol. Energy Mater. Sol. Cells*, 2010, **94**, 1618.
26. Z. Ma, Z. Tang, E. Wang, M. R. Andersson, O. Inganäs and F. Zhang, *J. Phys. Chem. C*, 2012, **116**, 24462.
27. C. Trinh, J. R. Bakke, T. P. Brennan, S. F. Bent, F. Navarro, A. Bartynski and M. E. Thompson, *Appl. Phys. Lett.*, 2012, **101**, 233903.
28. L. Y. Lin, Y. H. Chen, Z. Y. Huang, H. W. Lin, S. H. Chou, F. Lin, C. W. Chen, Y. H. Liu and K. T. Wong, *J. Am. Chem. Soc.*, 2011, **133**, 15822.
29. Y. H. Chen, L. Y. Lin, C. W. Lu, F. Lin, Z. Y. Huang, H. W. Lin, P. H. Wang, Y. H. Liu, K. T. Wong, J. Wen, D. J. Miller and S. B. Darling, *J. Am. Chem. Soc.*, 2012, **134**, 13616.
30. H.-W. Lin, H.-W. Kang, Z.-Y. Huang, C.-W. Chen, Y.-H. Chen, L.-Y. Lin, F. Lin and K.-T. Wong, *Org. Electron.*, 2012, **13**, 1925.
31. H.-W. Lin, C.-W. Lu, L.-Y. Lin, Y.-H. Chen, W.-C. Lin, K.-T. Wong and F. Lin, *J. Mater. Chem. A*, 2013, **1**, 1770.
32. M. C. Scharber, D. Mühlbacher, M. Koppe, P. Denk, C. Waldauf, A. J. Heeger and C. J. Brabec, *Adv. Mater.*, 2006, **18**, 789.
33. Y. Zhang, X.-D. Dang, C. Kim and T.-Q. Nguyen, *Adv. Energy Mater.*, 2011, **1**, 610.
34. H.-C. Yeh, H.-F. Meng, H.-W. Lin, T.-C. Chao, M.-R. Tseng and H.-W. Zan, *Org. Electron.*, 2012, **13**, 914.
35. J.-H. Chang, Y.-H. Chen, H.-W. Lin, Y.-T. Lin, H.-F. Meng and E.-C. Chen, *Org. Electron.*, 2012, **13**, 705.